Modelling carbon dioxide storage within closed structures in the UK Bunter Sandstone Formation

Williams, J.D.O.[a], Jin, M.[b], Bentham, M.[a], Pickup, G.E.[b], Hannis, S.D.[a] and Mackay, E.J.[b]

[a]*British Geological Survey, Environmental Science Centre, Keyworth, NG12 5GG, UK*
[b]*Institute of Petroleum Engineering, Heriot-Watt University, Riccarton Campus, Edinburgh, EH14 4AS, UK*

Abstract

The Bunter Sandstone Formation in the UK Southern North Sea has the potential to become an important CO_2 storage unit if carbon dioxide capture and storage becomes a widely deployed option for the mitigation of greenhouse gases. A detailed geological model of a region of the Bunter Sandstone consisting of four domed structural closures was created using existing seismic, well log and core data. Compositional simulation of CO_2 injection was performed to estimate the storage capacity of domes within the system. The injection was constrained by both pressure and CO_2 migration criteria, and the storage efficiencies of the domes (volume of stored CO_2 divided by the pore volume of the dome) were calculated when injection ceased. A sensitivity study evaluated the effect of varying the total aquifer volume, reservoir heterogeneity and injection well location. A wide range of storage efficiency values were obtained across the different simulation cases, ranging from 4% (closed dome) to 33% (homogeneous model). Intra-reservoir heterogeneity, specifically in the form of continuous low permeability layers has an important effect on storage capacity in dome-like structures, because it increases the tendency for CO_2 to migrate laterally from the storage complex via structural spill points.

Keywords Bunter Sandstone, Southern North Sea, Carbon dioxide, reservoir simulation.

1. Introduction

Despite environmental concerns about the long-term impacts of releasing vast quantities of CO_2 into the atmosphere, it is expected that the combustion of fossil fuels will continue to account for the majority of the world's energy needs in the foreseeable future (IPCC, 2005). Capturing CO_2 from large stationary emission sources such as power plants, and storing it in subsurface reservoirs is one of the tools that may be used to reduce greenhouse gas emissions, mitigating the impacts of global climate change while still allowing societies to meet their energy requirements. The Triassic Bunter Sandstone Formation of the UK sector of the Southern North Sea (SNS) is considered likely to have significant CO_2 storage potential (Holloway et al., 2006a, 2006b). It has fair to good reservoir properties as required for large-scale CO_2 storage in saline aquifers (Chadwick et al., 2008), and there is a regional seal immediately above it provided by the mudstones of the Triassic Haisborough Group. This seal is enhanced over much of the SNS by one or more of the three widespread but not ubiquitous halite members within the Haisborough Group. The stratigraphy and structure of the SNS are described in detail by Cameron et al. (1992) and Underhill (2003).

Structurally, the Bunter Sandstone contains several large periclines (henceforth referred to as Bunter domes) formed by post-depositional halokinesis in the underlying halite-dominated Zechstein Group. Many of the Bunter domes are faulted but, where satisfactorily sealed, they form structural traps that could immobilise and store significant quantities of injected CO_2. Some of the Bunter domes contain gas fields (Bifani, 1986; Ketter, 1991; Ritchie and Pratsides, 1993), which demonstrates (a) the ability of the Bunter Sandstone to store buoyant fluids, and (b) that, at least where unfaulted, the overlying strata are capable of sealing significant gas accumulations. The non-gas-bearing domes are saturated with highly saline brine.

Previous studies of the CO_2 storage potential of the Bunter Sandstone indicate that more detailed appraisals are needed to obtain more realistic estimates of its capacity to store CO_2 (Bentham, 2006; Holloway et al. 2006a). Hence this study investigates the storage potential of one of the Bunter domes in detail using geocellular models and reservoir simulation.

2. Methodology and geocellular modelling

The aims of the study were to examine the likely storage efficiency and storage capacity by (1) simulating the injection of realistic industrial quantities of CO_2 into a single Bunter dome, (2) investigating potential pore fluid pressure and hence injectivity interactions resulting from injection into multiple domes, and (3) investigating the sensitivity of injection to a range of boundary conditions and other uncertain parameters. The following methodology was used:

- Selection of an appropriate region containing a number of structurally prospective domes.
- Static geological modelling to provide a geocellular framework for property attribution and dynamic simulation.
- Detailed reservoir characterisation of the Bunter Sandstone in the model region, including the identification of key features likely to affect storage behaviour and efficiency.
- Determination of the petrophysical property distribution for the base case model based on the above.
- Base case dynamic model simulation in order to calculate the storage efficiency of a single dome (E_d).
- Sensitivity analysis and examination of boundary conditions and other parameters that could affect the storage efficiency of the Bunter domes.

2.1. Selection of the model region

A static geological model of a volume of the Bunter Sandstone containing four domes was constructed (Fig. 1). The dome containing well 44/26–01 (henceforth Dome A) was selected as the primary focus of the study because it meets the following criteria:

- It falls near the middle of the size range for the Bunter domes.
- It has considerable topographical relief between its crest and spill-point, providing significant structural closure.

- No seismically resolvable faults have been identified within the area of structural closure that cut the top Bunter Sandstone and the full Haisborough Group seal (Fig. 2).
- The crest of the dome is at a suitable depth for CO_2 storage (approximately 1186 m sub-sea).

The dome is located near to three other domes (Fig. 1) that were included in the model so that potential pressure interference effects could be investigated. The structure of most of the modelled area, and the entirety of Dome A, is well imaged by 3D seismic data (Fig. 2). Minor faulting affects at least one of the adjacent domes (Dome B), thought to be caused by extensional stresses related to the development of the underlying salt dome. These faults were not included in the model because the throws of the faults are relatively minor compared to the overall seal thickness.

2.2. Structural modelling

A geocellular model was built using Schlumberger's proprietary PETREL software. Depth converted surfaces covering most of the modelled area for the top Chalk Group, Base Cretaceous Unconformity, top Triassic and top Bunter Sandstone Formation were utilised, interpreted by PGS from their SNS MegaSurvey 3D seismic dataset. The surfaces were interpolated across areas not covered by the seismic data. The seismically derived structural surfaces were validated against well data, and well formation tops were used to provide further stratigraphic zonation. Fig. 3 illustrates the stratigraphic subdivision of the model area in the UK SNS.

The overlying seal, the Haisborough and Penarth Groups (43–826 m thick over model area), were divided into the Solling Claystone, which lies directly above the Bunter Sandstone, the Röt Halite Member and the Upper Haisborough Group (interbedded mudstone, halite and anhydrite), which for the purposes of this study includes both the Penarth and remaining Haisborough Group. These divisions within the Haisborough Group were isopached from well data and gridded conformably to the top Bunter Sandstone surface. The reservoir itself is the Bunter Sandstone, its thickness ranging from 174–274 m, with an average thickness of 225 m. The immediately underlying strata, forming the bottom seal, consist of the Triassic Bunter Shale Formation, the base of which forms the base of the model.

Five intra-reservoir zones were recognised within the Bunter Sandstone and correlated on wireline logs throughout the modelled area. Each zone was layered at a resolution appropriate to capture the principal intra-zone variations observed on the geophysical logs. In order to more accurately model CO_2 buoyancy effects, cells towards the top of the reservoir and below widespread impermeable horizons are thinner, enabling better imaging of the evolving distribution of CO_2 during the dynamic modelling. Within the reservoir interval, the thinnest cells in the model are 0.56 m thick, while the average cell thickness is 3.9 m. The simulation model consists of 429,660 active grid cells with a horizontal increment of 400 x 400 m; the horizontal cell dimensions are the result of the need to compromise between the requirement to incorporate fine-scale vertical layering whilst maintaining reasonable simulation run times.

2.3. Reservoir description

The five Bunter Sandstone reservoir zones were identified from geophysical logs, primarily gamma ray (GR), sonic (DT) and bulk density (RHOB) curves. They occur throughout the modelled area, and are broadly comparable in terms of their lithofacies and log character to reservoir zones identified by Ketter (1991) in the Esmond, Forbes and Gordon gas fields and by Ritchie and Pratsides (1993) in the Caister B gas field. Depositional environments were interpreted for each reservoir zone based on petrophysical properties and a regional depositional model for the Bunter Sandstone (Table 1). The succession is dominated by sheetflood sandstones and fluvial clastic sediments deposited on an alluvial braidplain (Ritchie and Pratsides, 1993). Channels and streams are believed to exhibit a low sinuosity, with sediment sourced from the London-Brabant Massif and Pennine High to the southwest (Cameron et al., 1992). Ritchie and Pratsides (1993) proposed the fluvial system drained into a playa lake to the northeast of Caister B. In the Esmond, Forbes and Gordon gas field complex to the north, the Bunter Sandstone represents a series of coalescing alluvial fans dissected by braided fluvial channels deposited in an arid to semi-arid environment (Bifani, 1986).

The porosity of the reservoir is strongly influenced by rapid variation in lithology and the degree and type of cementation. Varying quantities of dolomite, halite and anhydrite cements are observed in the Bunter Sandstone (Ketter, 1991).

Within the zones are several cemented sandstone layers (Table 1) identified by a low gamma ray response, together with a sharp increase in both sonic velocity and bulk density. Of particular note is the distinct cemented sandstone layer at the top of Zone 4 which can be observed in all but two of the wells in the model area and outside the modelled area up to distances of 20 km to the northeast, in the Caister B gas field (well 44/23–1). Interpretation of the geophysical logs and petrographic analysis from well 44/23–1 indicate an abundance of cement within the coarse grained sandstone (Fig. 4).

3. Reservoir properties

3.1. Lithological modelling

The reservoir was divided into three lithology categories on the basis of petrophysical analysis; non-cemented sandstone, cemented sandstone (sandstone with occluded porosity) and shale.

A discrete lithofacies log was generated for each well in order to upscale lithology into the model grid (Fig. 5). These logs were upscaled to the 3D grid, and distributed throughout each reservoir zone in the model in accordance with the reservoir description for each zone (Fig. 6). The degree of upscaling is apparent from Fig. 5. Some of the thinner lithological units have been omitted, while the thickness of others have been increased by the upscaling process.

Lithofacies were distributed within each of the reservoir zones using a combination of deterministic and stochastic modelling techniques (Table 2). These include log correlation, object modelling and Truncated Gaussian Simulation (Deutsch and Journel, 1992). In each zone the distribution honoured that observed in the well logs and interpreted vertical and lateral trends in the regional depositional environment.

The cemented sandstone layer at the top of Zone 4 is present in all but two wells in the model region, but its lateral continuity is uncertain. Sensitivity to the continuity and permeability of this layer was investigated in the dynamic simulations.

3.2. *Base Case petrophysical modelling*

Porosity logs were calculated and upscaled for the non-cemented sandstones using geophysical logs, and a porosity distribution was stochastically generated through the reservoir interval using Sequential Gaussian Simulation (SGS). The distribution honours that of the upscaled porosity log data and lies within a range of 5–35% established from regional core data. The resultant porosity realisation for the non-cemented sandstone exhibits a normal distribution with a mean porosity of 18%.

Very few permeability data exist within the model area due to the scarcity of core and production data from the Bunter Sandstone. Permeability was therefore assigned to the model using bivariate SGS, where the distribution of permeability is dependent on the values of porosity simulated previously in the grid. The correlation between porosity and permeability for the non-cemented sandstone was derived from analysis of the relationship as seen from core data taken from all Bunter Sandstone core in the UK sector SNS available to this study (Fig. 7). A wide-range of permeability values were given (0.001–15,000 mD), while the arithmetic mean permeability of all the non-cemented sandstone lithology cells is 248 mD, and the geometric mean is 30 mD.

Little reliable information is available from core on the porosity and permeability of shale within or immediately above or below the Bunter Sandstone in the UK sector. As a consequence, porosity and permeability of the intra-Bunter Sandstone shales, the Bunter Shale Formation and Haisborough Group were assigned constant values of 3% and 6.5×10^{-3} mD respectively. These are rounded averages of values given by Spain and Conrad (1997) for the Solling Claystone in the Dutch sector. Quantitative analysis of top-seal capacity in the Dutch Sector suggests that, at least where laterally continuous, the Solling Claystone and Röt Halite Member form an effective top-seal (Spain and Conrad, 1997).

The thin, dense, high-velocity layer at the top of Zone 4 observed on the logs is thought to have very low porosity due to occlusion of the pore space by cement. This is suggested by the significant density contrast observed on the geophysical logs between cemented and un-cemented sandstones, and is supported by observations of cemented sandstone intervals in core from well 44/23–1 (Fig. 4). In the base case model, the porosity was set to 1×10^{-5} and the permeability was given the same value as the shale (6.5×10^{-3} mD). Cases with modified porosity and permeability values were also tested as described in the sensitivity case studies (Section 5.2).

3.3. Additional data for simulation models

Additional data used in the simulations are listed in Table 3. Much of the data was obtained from the ETI UK SAP project (Gammer et al., 2011).

No relative permeability or capillary pressure measurements for CO_2/brine were available in the region modelled for this study, therefore measurements from Bennion

and Bachu (2006, 2008) Viking 2 curves were used for the sandstone, and their Calmar values were used for the shale.

In the absence of site specific data, a fracture pressure gradient of 0.018 MPa/m (0.8 psi/ft) was assumed. This was chosen as a typical value reported for formations beneath the North Sea (Wiprut and Zoback, 2000; Wiprut, 2001), and is close to the fracture pressure gradient given by Noy et al. (2012).

4. Reservoir simulations

The primary aim of the reservoir simulation was to determine the storage capacity of Dome A, given imposed limitations to pressure build-up and migration out of the dome via its structural spill-points. The pressure controls and the spill-points are described in Sections 4.2 and 4.3, respectively.

A base-case dynamic simulation of CO_2 injection into Dome A was performed, followed by a sensitivity study which focussed on the effect of varying the model boundary conditions, connected aquifer size, heterogeneity and injection strategy in order to assess their effect on storage capacity. The sensitivity analyses are described in Sections 5 and 6, while the full-range of results are summarised in Tables 5 and 6 (Section 7).

In each simulation the dome storage efficiency, E_d, was calculated, which is defined as:

$$E_d = \frac{\text{Volume of } CO_2 \text{ Injected (at reservoir conditions)}}{\text{Total Pore Volume of Dome}} \quad (1)$$

The Total Pore Volume of each dome was calculated from the geocellular model, by determining the pore volume above the respective spill-points.

Dynamic simulation was performed using the ECLIPSE 300 reservoir simulator, with the CO2STORE module (Schlumberger, 2010) which allows for simulating the mutual solution of CO_2 and brine.

4.1. The Base Case

In the base case model, injection of CO_2 into Dome A (Figs. 1 and 2) was simulated. It was assumed that pure CO_2 would be supplied from a power station to the storage site at a maximum rate of 20 Mt/yr. Ten vertical wells were used with an initial injection rate of up to 2 Mt/yr/well, with perforations in each of the sandstone layers in Bunter Sandstone zones 1–4 (Zone 5 was not utilised for injection because of the high shale content of its upper layer). The objective here was to examine the storage efficiency of the dome and the resulting pressure effects, rather than to optimise well injection scenarios. It was deemed that ten wells would be necessary to inject the volume of CO_2 potentially supplied by either a single large power station or cluster of industrial emission sources. The wells were positioned in a regular circular configuration around the crest of the dome along a constant depth contour. Therefore, well location was not optimised based on the permeability distribution. The depth of the uppermost perforations in the wells of the base case model was 1300 m. The

sensitivity to the well positioning, in terms of the optimum depth contour of the uppermost perforations was examined and is discussed later.

4.2. Control of injection wells

Although the wells were initially controlled by injection rate (2 Mt/yr/well), the injection of CO_2 was constrained by pressure build-up. The allowable bottom-hole pressure (BHP) was set to 90% of the fracture pressure, with an assumed fracture pressure gradient of 0.018 MPa/m (0.8 psi/ft). If pressure rose above the BHP limit in any well, the injection rate of that well was reduced so that this limit was not exceeded (Fig. 8). A monitoring well was placed at the crest of each dome to monitor pressure build-up, because the crest of a dome is critical for two reasons. Firstly, CO_2 will theoretically accumulate in this vicinity, increasing the pressure, and secondly, the fracture pressure is lower at the shallowest point of the structure. Additionally, but not explicitly considered here, the crest of the domes represent the zone of maximum flexure and are therefore more likely to exhibit fracturing. The simulations were configured so that the injection rate for each injector within the dome was reduced by 20% if the BHP of the monitoring well exceeded its maximum allowable value (90% of the fracture pressure at that depth). In the base case simulation, the limit for the injection well BHPs was 210 bars, while that for the crestal monitoring well was 200 bars. The cumulative injection rate over time is shown in Fig. 8, and documents an overall reduction with time. The modelling presented here assumes a non-constant rate of CO_2 supplied for storage.

4.3. Spill point criterion

In the simulations, the migration of CO_2 out of the designated storage complex via the dome spill-points was monitored (we are assuming that observation wells and/or geophysical monitoring tools may be used to detect the presence of CO_2 at the spill-points). In this study, the storage complex was defined as the structural closure of the dome (or domes) into which injection was taking place. A criterion was set for the maximum allowable spillage from a dome. This limit was initially set at a conservative level of 0.01% of the injected CO_2 by mass (including both free and dissolved CO_2). This may seem a low level; however, it was noted that once CO_2 was detected at the spill point, the concentration could rise rapidly. The effect of increasing the spillage criterion is addressed later in the discussion. The spill point for each dome was determined from the geological model, and hence the pore volume of the Bunter Sandstone interval (excluding Zone 5 due to its high shale content) was calculated for each dome. Note that the spill point depth for the domes varied in different injection scenarios, as shown in Fig. 9. If only Dome A was used to store CO_2, the spill point depth was 1730 m (Fig. 9a), whereas if Domes B and D were included in the storage complex the spill depth was 1760 m (Fig. 9b).

The effective injection time was the time taken for the spill criterion to be reached, while the capacity of the dome was the total volume of injected CO_2 in that time period. If the spill point was not breached after a period of 50 years, injection was ceased. This limit was set because the lifetime of a power station is likely to be somewhat less than this. Also, it should be noted that it is possible to increase the capacity of a storage site by injecting at a lower rate over a given time period.

4.4. Base Case model boundary conditions

Saline aquifers are often very large, covering hundreds of km^2, and it is currently not feasible to model the whole formation in detail. Modelling is therefore focussed on the region affected by the CO_2 plume. However, the pressure footprint due to injection extends much further (Noy et al., 2012; Smith et al., 2010), requiring pressure dispersal within the connected aquifer to be considered in order to avoid unrealistic pressure build-up within the model. In this study, we assumed an initial connected aquifer volume of 280 km^3 (from initial estimates made during the ETI UK SAP study). The pore volume of the geocellular model was 40 km^3, and the additional volume was accounted for using numerical aquifers surrounding the model. A major uncertainty is the size of the connected aquifer pore volume and this was addressed in the sensitivity studies. The pore volume above the spill point of Dome A, which was used when estimating the storage efficiency, was 2.542×10^9 m^3.

4.5. Base Case modelling results

In the base case simulation, the pressure built up rapidly in some wells and the injection rate was reduced accordingly. The spillage criterion was reached after 20 years of injection, and within this time the pressure in the monitoring well did not reach the limiting pressure. However, if injection was continued beyond this time, the pressure in the monitoring well would reach the maximum allowable limit, even though the injection rates in the injection wells were already limited by their BHP. This demonstrates that monitoring the pressure at the crest of a dome is important to ensure that caprock integrity is maintained.

The limiting factor for CO_2 storage in the base case model was therefore a combination of pressure build-up and CO_2 migration. After 20 years of injection, the dome storage efficiency, E_d, was 19.1%, corresponding to a CO_2 storage capacity of 331 Mt.

5. Parameter sensitivity analysis

Due to a lack of site-specific data many of the parameters in the geological model are uncertain. To deal with the uncertainty, two sets of sensitivity studies were carried out based on aquifer size and heterogeneity.

5.1. Aquifer size

The base case model assumed that the volume of the connected pore space was 280 km^3. It is known that the Bunter Sandstone outcrops at, or very near to, the sea bed less than 20 km from the model at well 43/28a–3. If this is considered, the pore volume could be regarded as being very large, as the seabed outcrop may provide a means of pressure relief for the open aquifer (Noy et al., 2012). To mimic the effect of a potentially very large aquifer, the pore volume of the surrounding aquifer was multiplied by 1000. In addition, simulations were undertaken in which (1) the model boundaries were closed and (2) Dome A itself was closed. These models are referred to as follows:

- Base case with an aquifer pore volume of 280 km^3 ("Base-Case").

- Open model with an aquifer volume of 24,293 km^3 ("Open").
- Model boundaries closed, corresponding to an aquifer pore volume of 40 km^3 ("Closed").
- Dome boundaries closed, corresponding to an aquifer pore volume of 12 km^3 ("Closed Dome").

The terms in brackets refer to the simulation case names in Table 5.

The storage efficiency results for Dome A are shown in Fig. 10. As expected, the storage efficiency decreases as the size of the aquifer is reduced, due to pressure build-up. However, in the open aquifer boundary case, the dome storage efficiency was less than in the base case as the pressure was able to diffuse readily from the wells so that the injection rate could be maintained, resulting in CO_2 migrating more rapidly towards the spill point. This demonstrates the importance of considering CO_2 migration together with pressure as constraints on CO_2 storage capacity, and that it may be necessary to make a compromise between achieving the desired injection rate and maximising storage capacity.

5.2. Heterogeneity

There is much uncertainty in the petrophysical properties of the geological model. Although the cemented sandstone layer at the top of reservoir Zone 4 appears in most wells in the model area, it is known that it is not ubiquitously continuous across the region as it does not occur in at least two of the wells. Therefore a model case where this layer was removed was simulated ("No Cem Layer" in Table 5). The layer was effectively removed by substituting its petrophysical properties with those from the layer directly beneath it. Fig. 11 demonstrates the effect of the cemented layer on the CO_2 distribution in the layer immediately below, comparing cases with and without it. Note that the presence of the impermeable cemented layer promotes migration of CO_2 towards the spill-point into Dome B, whereas this does not occur if this layer is removed. This is due to the CO_2 migrating upwards due to buoyancy, and spreading beneath the impermeable layer towards the spill point. When the cemented layer is removed the CO_2 migrates unimpeded to the crest of the dome and therefore it has more contact with the reservoir, increasing the storage efficiency as shown in Fig. 12. As the petrophysical properties of the cemented sandstones and shale were uncertain, these were modified during the sensitivity analysis as shown in Table 4. The high and low permeability cases are labelled "Ksh&cem hi" and "Ksh&cem lo" in Tables 4 and 5.

In addition, sensitivity to the k_v/k_h ratio (the ratio of vertical to horizontal permeability) was examined. In the base case, $k_v/k_h = 1$, while sensitivity cases used $k_v/k_h = 0.1$ and 0.01. These cases are labelled "Kv/kh 0.1" and "Kv/kh 0.01" in Fig. 12 and Table 5. A final heterogeneity sensitivity case was considered using a homogenous model with a porosity of 15% and permeability of 100 mD ("Homo"). The results are summarised in Fig. 12, and listed in Table 5.

These results show that the storage efficiency decreased with decreasing k_v/k_h ratio. This is because the reduction in vertical permeability causes an increase in pressure build-up at the wells resulting in reduction of the injection rate. Note that this result

differs from the results of Gorecki et al. (2009), who found that the storage efficiency increased with a decrease in k_v/k_h due to the effect of buoyancy reduction, resulting in a thicker plume. This difference reflects slight differences in methodology for estimating storage efficiency, and also demonstrates that some factors influencing CO_2 storage are model-dependent.

The highest storage efficiency in the sensitivity studies was obtained from the homogeneous case. Here the lack of heterogeneity allowed the CO_2 to migrate upwards, slowing the movement towards the spill point and increasing the trapping potential of the dome structure. Varying the porosity and permeability of the cemented sandstone and the shale lithologies had little effect because the majority of these low permeability layers are not laterally continuous (Fig. 6).

6. Effect of injection strategy

Section 5 described sensitivity analyses aimed at addressing the uncertainty of poorly defined parameters. Other factors which affect the CO_2 storage efficiency such as well completion depth, and the number of domes utilised by the storage complex were also investigated. These cases utilise the base case model parameters.

6.1. Depth of well completions

The depth to the topmost well completions in the base case simulation was 1300 m, somewhat deeper than the depth to the crest of Dome A which lies at ~1200 m. The depth of the shallowest spill point is 1730 m, and so cases were investigated with the well completions at 1200 m, 1450 m and 1600 m (Fig. 13). These cases are referred to as "W1200", "W1450" and "W1600" in Table 5. In the 1200 m case (crest of Dome A), nine wells rather than ten were arranged around the crest of the dome in order to maintain a suitable well spacing, yet the total initial injection rate remained the same. The pressure built up rapidly, leading to a reduction in injection rate. However, injection continued for 50 years and the spillage criterion was not reached in this time, resulting in a high storage efficiency of 28.7%. Conversely, injection at the crest would be considered a high risk strategy, as drilling the crest may compromise storage integrity and there may be existing fractures in the caprock susceptible to reactivation. This case is therefore not considered to be realistic, and is distinguished by hatching in Fig. 13b. In the other cases, the deeper wells resulted in the CO_2 reaching the spill point sooner, decreasing the storage efficiency. Fig. 13b shows the effect of injection well depth on the storage efficiency of Dome A.

6.2. Storage in multiple domes

The pressure footprint caused by CO_2 injection reaches far beyond the extent of the CO_2 plume (Heinemann et al., 2012; Smith et al., 2010; Noy et al., 2012). Moreover, in this study, results show that tens of years may pass before the formation pressure recovers after injection has ceased. The pressure recovery time depends on a number of factors, including the boundary conditions and the pressure diffusivity, which in turn depends on the permeability, fluid viscosity and compressibility. Fig. 14 illustrates the build-up of pressure in Dome B due to injection in Dome A. Clearly the capacity of Domes B and D will be affected by injection into Dome A.

Several cases were performed in order to assess the sensitivity of the storage capacity to injection in multiple domes. These simulations used the same petrophysical properties and boundary conditions as the base case. Using Domes A, B and D, scenarios included injection into two or three of the domes, and also the effect of injecting into separate structures both simultaneously and sequentially. Here we compare single-dome injection with injection into three domes. As only part of Dome C was included in the model, it was not considered for injection. Injection was via ten wells in each dome, with an initial target rate of 2Mt/yr/well. For Dome A, the depth of the well completions was the same as in the base case, and appropriate depths were chosen for the completions of the wells in the other domes. As in the base case, the wells were limited by the BHP of each injection well and the pressure in a monitoring well positioned in the crest of each dome. Injection in each dome was also constrained by the spillage criterion. For the multi-dome simulations, the total simulation time was 100 years, compared with 50 years for the single dome case. The storage efficiency for each dome in each case was calculated, and the results were averaged using the pore volume of the domes as a weighting factor.

The results are summarised in Table 6 and Fig. 15, where "A+B+D" refers to simultaneous injection into the three domes and "A/B/D" refers to injection in series. The single dome results are also shown for comparison. The case "A only" represents the base case. Dome B had the lowest storage efficiency because the spill point was reached soonest, after 12 years of injection. In Dome D, the spillage criterion was not reached for 26 years, and a greater mass of CO_2 was stored (Table 6). However, Dome D has a larger pore volume than Dome A and therefore the storage efficiency was lower. The multi-dome cases both had average dome storage efficiencies that were lower than the storage efficiency for Dome A, E_d for the sequential case being lower than E_d for the simultaneous case. It is expected that the efficiency will decrease when injecting into multiple domes due to pressure build-up. Here we also considered spillage and the time taken for CO_2 to reach a spill point, which depends on a number of factors, such as the depth of spill point and the reservoir permeability. These factors vary from dome to dome, so there was not a clear trend in E_d and the number of domes used for injection, or whether the domes were used simultaneously or in sequence.

7. Results of the sensitivity studies

Results of all the sensitivity cases are summarised in Tables 5 and 6, which list the results for the single-dome sensitivity study and the multi-dome study respectively. In addition to showing the storage efficiency, the tables also give the time taken for 0.01% of the injected CO_2 by mass to reach the spill point (spill time) and they list the CO_2 storage capacity, taken as the total mass of CO_2 stored. There is a wide variation in the storage efficiency throughout the sensitivity studies. E_d ranges from 4% (closed dome) to 33% (homogeneous model). Across the simulations described here, between 0.1% and 0.8% of the total aquifer volume is utilised for storage, but this does not constitute a measure of the storage capacity for the whole aquifer because the simulations are focussed on specific domes.

8. Discussion

The results presented here show that the derived storage efficiency depends on the aquifer size, the heterogeneity, well positioning and the injection strategy. The simulations indicate that it may be possible to increase storage capacity by controlling the ratio of viscous/gravity forces acting on the CO_2. If the injection rate is high (high viscous force), the pressure will rise, necessitating a reduction of the injection rate. Alternatively, if the limiting pressure is not reached, the CO_2 may rapidly migrate towards a spill point. On the other hand, a lower injection rate (low viscous/gravity ratio) will encourage the buoyant rise of CO_2 and also the dissolution of CO_2 in brine, increasing the storage capacity, but possibly meaning that the injection rate required for contractual reasons cannot be achieved.

There are a number of other factors which can significantly affect the results. The criteria used for controlling the simulation have a significant effect. In the simulations described above, it was assumed that the fracture pressure gradient was 0.8 psi/ft (0.018 MPa/m). However, cases using a reduced fracture pressure gradient of 0.7 psi/ft reached the pressure limit sooner, leading to a reduced injection rate. This allows the CO_2 to rise buoyantly and delays migration towards the spill point, leading to a higher storage efficiency.

Another factor which affects the results is the criterion used for spillage. In this study, injection was ceased when 0.01% of the CO_2 (by mass) had crossed the spill point. If this is changed to 1%, the storage capacity will evidently increase in the cases which are limited by spillage (i.e. in all cases with the exception of the closed model and closed dome). In most of the cases with injection into Dome A, the storage efficiency approximately doubled. For example, in the base case, E_d increased from 19.1% to 35.6%. When the cases were ordered in terms of storage efficiency values, there was little change in the order when the spillage level was increased. There were three exceptions:

- The W1600 model (wells at a depth of 1600 m) fared better with the high spillage level because of the increased well spacing, and due to the wells being closer to the spill point. Increasing the spillage level to 1% increased the E_d by a factor of 2.7.
- E_d for the W1200 model (wells at the crest) barely changed, because the capacity was largely controlled by pressure. Spillage did not reach the 0.01% level until 46 years (Table 5), and injection was continued for 50 years when the spillage level was 1%.
- E_d for the homogeneous model only increased by a factor of 1.3, because the CO_2 injection rate was lower in this model, due to pressure constraints. The buoyant rise of CO_2 was not hampered by low permeability layers, leading to pressure build-up in the crest of the structure, resulting in a reduction of the injection rate.

It should also be noted that when the limit was set to 1%, the values obtained for the storage efficiency approached the value of 40% assumed by Bentham (2006) for static capacity estimation.

The EU directive (European Parliament, 2009) states that ‘the selection of the appropriate storage site is crucial to ensure that the stored CO_2 will be completely and

permanently contained'. As a result, models will be required to predict the movement of CO_2 out of the storage complex and to help identify risk factors such as migration pathways, for example spill points which may lead to lateral migration from the storage site. For storage sites where the spill points pose a significant risk to leakage of CO_2 out of the storage complex it may be prudent to include adjacent structures in the leased storage complex. This may be particularly important for storage sites with high permeability pathways or anisotropy that may lead to rapid CO_2 migration towards particular spill points.

The issue of pressure vs migration in constraining CO_2 storage capacity has been studied by Szulczewski et al. (2010). They derived analytical equations for constraints in capacity, assuming a simple tilted model, and determined that with short injection time-scales, storage capacity was likely to be pressure-limited in large shallow reservoirs, with low permeability and high porosity. The present study focused on domed structures and included the effects of geological heterogeneity. In this case the results show that storage capacity is likely to be pressure-dominated in small aquifers (as one would expect) and in cases where CO_2 is injected close to the crest. On the other hand, the capacity is likely to be migration-dominated in large aquifers with low k_v/k_h, or when horizontal low permeability barriers are present (assuming injection away from the crest).

Finally, it is well known that grid resolution is a problem in numerical simulations concerning CO_2 storage (Pickup et al., 2010). If the grid is too coarse it may lead to an underestimation of the plume migration distance. Additionally, there will be an overestimation of the volume of CO_2 which dissolves, because more CO_2 will dissolve in a larger grid cell and the increase in pressure will be underestimated. Current work is addressing the issue of the optimum grid resolution for different processes which arise during CO_2 storage (Jin et al. 2012; Pickup et al. 2012).

9. Summary and conclusions

In this study a detailed geological model of part of the Bunter Sandstone Formation has been generated in order to estimate the CO_2 storage efficiency of domed structural closures using numerical simulations. The geological model allowed an evaluation of the effects of reservoir heterogeneity on the storage efficiency, which is important for understanding the factors affecting geological storage of CO_2.

The injection of CO_2 was carefully controlled in the simulations, using pressure control at the wells, and in a monitoring well at the crest of the dome(s). Migration of CO_2 away from the injection wells was monitored, and injection ceased when a specified proportion of the injected CO_2 passed the spill points. These controls on the injection produced lower estimates of CO_2 storage efficiency than some previous studies. For example, the dome storage efficiency (E_d) for the base case model was 19%, compared with the 40% assumed by Bentham (2006). A key assumption is that maintaining a constant injection rate is not considered a requirement during the modelling. This study therefore assumes that any CO_2 not injected due to the imposed pressure constraints, would need to be diverted elsewhere for storage.

In summary, the volume of CO_2 which may be stored in a given formation is governed by a complex interaction between the reservoir heterogeneity, and the balance of viscous and gravity forces.

Notable results from this study were:

- When injecting into structural closures such as domes in the Bunter Sandstone, the CO_2 storage capacity of large open aquifers is not necessarily greater than in closed or partially closed aquifers when spillage is taken into consideration.
- It is important to consider the build-up of pressure at the crest of a dome, where the critical pressure limit may be reached before the fracture pressure is attained at the depth of the well connections.
- When injecting CO_2 into a closed structure such as a dome it is important to assess the continuity of low permeability layers, because this significantly affects whether CO_2 will preferentially rise buoyantly to the crest of the structure, or migrate towards a spill point.

The last result re-iterates that thorough site characterisation is a vital requirement before CO_2 storage is undertaken in any formation.

Acknowledgements

This study was carried out as part of the UK Storage Appraisal Project, commissioned and funded by the Energy Technologies Institute. We would like to thank the Energy Technologies Institute for permission to publish this work, and the project consortium for their input. The authors would also like to thank PGS for use of the 3D seismic data and interpretation used in this study, and for the use of their data in the images published in this paper. We thank Schlumberger for the use of the PETREL and ECLIPSE software. Foundation CMG is thanked for funding the Chair in Reactive Flow Simulation held by Eric Mackay. The BGS authors publish with the permission of the Executive Director, British Geological Survey (NERC).

References

Bennion, D.B., Bachu, S., 2006. The Impact of Interfacial Tension and Pore-Size Distribution/ Capillary Pressure Character on CO_2 Relative Permeability at Reservoir Conditions in CO_2-Brine Systems. SPE 99326, presented at the SPE/DOE Symposium on Improved Oil Recovery, Tulsa, Oklahoma, 22–26 April, 2006.

Bennion, D.B., Bachu, S., 2008. Drainage and Imbibition Relative Permeability Relationships for Supercritical CO_2/Brine and H_2S/Brine Systems in Intergranular Sandstone, Carbonate, Shale and Anhydrite Rocks. SPE 99326, SPE Reservoir Evaluation and Engineering 11 (3), 487–496.

Bentham, M., 2006. An assessment of carbon sequestration potential in the UK – Southern North Sea case study. Tyndall Centre for Climate Change Research, Working Paper 85.

Bifani, R., 1986. Esmond Gas Complex. In: Brooks, J., Goff, J.C., Van Hoorn, B. (Eds.), Habitat of Palaeozoic Gas in N.W. Europe. Geological Society, London, Special Publications 23, 209–221.

Cameron, T.D.J., Crosby, A., Balson, P.S., Jeffery, D.H., Lott, G.K., Bulat, J., Harrison, D.J., 1992. The Geology of the Southern North Sea. United Kingdom Offshore Regional Report. British Geological Survey and HMSO, London.

Chadwick, R.A., Arts, R., Bernstone, C., May, F., Thibeau, S. and Zweigel, P., 2008. Best Practise for the Storage of CO_2 in Saline Aquifers. British Geological Survey, Keyworth, Occasional Publications 14.

Deutsch, C.V., Journel, A.G., 1992. GSLIB: Geostatistical Software Library and User's Guide. Oxford University Press, New York.

European Parliament, 2009. EU Directive 2009/31/EC – The Geological Storage of CO_2. Retrieved April 2011, from The European Parliament and The Council of The European Union, Europa Website [http://eur-lex.europa.eu/Notice.do?val=496647:cs&lang=en&list=496647:cs,&pos=1&page=1&nbl=1&pgs=10&hwords=&checktexte=checkbox&visu=#texte].

Gammer, D., Green, A., Holloway, S., Smith, G., 2011. The Energy Technologies Institute's UK CO_2 Storage Appraisal Project (UKSAP). SPE 148426, presented at the SPE Offshore Europe Oil and Gas Conference and Exhibition, Aberdeen, UK, 6–8 September, 2011.

Gorecki, C.D., Sorensen, J.A., Bremer, J.M., Knudsen, D.J., Smith, S.A., Steadman, E.N., Harju, J.A., 2009. Development of Storage Coefficients for Determining the Effective CO_2 Storage Resource in Deep Saline Formations. SPE 12644, presented at the SPE International Conference on CO_2 Capture, Storage, and Utilization, San Diego, 2–4 November, 2009.

Heinemann, N., Wilkinson, M., Pickup, G.E., Haszeldine, R.S., Cutler, N.A., 2012. CO_2 Storage in the offshore UK Bunter Sandstone Formation. International Journal of Greenhouse Gas Control 6, 210–219.

Holloway, S., Vincent, C.J., Bentham, M.S., Kirk, K.L., 2006a. Top-down and bottom-up estimates of CO_2 storage capacity in the United Kingdom sector of the southern North Sea basin. Environmental Geosciences 13, (2), 71–84.

Holloway, S., Vincent, C.J., Kirk, K.L., 2006b. Industrial carbon dioxide emissions and carbon dioxide storage potential in the UK. DTI Report COAL R308. DTI/Pub URN 06/2027, DECC, London.

IPCC, 2005. IPCC Special Report on Carbon Dioxide Capture and Storage. Working Group III of the Intergovernmental Panel on Climate Change. In: Metz, B., Davidson, O., de Coninck, H.C., Loos, M., Meyer, L.A. (Eds.), Cambridge University Press, Cambridge.

Jin, M., Mackay, E., Akhurst, M., Hitchen, K. and Quinn, M., 2012. Evaluation of the CO_2 Storage Capacity of the Captain Sandstone Formation. SPE 154539, presented at the EAGE/SPE Europec Conference and Exhibition, Copenhagen, Denmark, 4–7 June, 2012.

Ketter, F.J., 1991. The Esmond, Forbes and Gordon Fields, Block 43/8a, 43/13a, 43/15a, 43/20a, UK North Sea. In: Abbotts, I.L. (Ed.), United Kingdom Oil and Gas fields, 25 Years Commemorative Volume, Geological Society, London, Memoirs 14, 425–432.

Noy, D.J., Holloway, S., Chadwick, R.A., Williams, J.D.O., Hannis, S.A., Lahann, R.W., 2012. Modelling large-scale carbon dioxide injection into the Bunter Sandstone in the UK Southern North Sea. International Journal of Greenhouse Gas Control 9, 220–233.

Pickup, G.E., Kiatsakulphan, M., Mills, J.R., 2010. Analysis of Grid Resolution for Simulations of CO_2 Storage in Deep Saline Aquifers. Presented at the 12th European Conference on the Mathematics of Oil Recovery, Oxford, UK, 6–9 September, 2010.

Pickup, G.E., Jin, M., Mackay, E.J., 2012. Simulation of Near-Well Pressure Build-up in Models of CO_2 Injection, presented at the 13th European Conference on the Mathematics of Oil Recovery, Biarritz, France, 10–13 September, 2012.

Ritchie, J.S., Pratsides, P., 1993. The Caister fields, Block 44/23a, UK North Sea. In: Parker, J.R. (Ed.), Petroleum Geology of Northwest Europe: Proceedings of the Fourth Conference, Geological Society, London, 759–769.

Schlumberger, 2010. Eclipse 300 Technical Manual.

Smith, D.J., Noy, D.J., Holloway, S., Chadwick, R.A., 2010. The Impact of Boundary Conditions on CO_2 Storage Capacity Estimation in Aquifers. Energy Procedia 4, 4828–4834.

Spain, D.R., Conrad, C.P., 1997. Quantitative analysis of top-seal capacity: Offshore Netherlands, Southern North Sea. Geologie en Mijnbouw 76, 217–226.

Szulczewski, M.L., MacMinn, C.W. and Juanes, R., 2010. How Pressure Buildup and CO_2 Migration Can Both Constrain Storage Capacity in Deep Saline Aquifers. Energy Procedia 4, 3904–3910.

Underhill, J.R. 2003. The tectonic and stratigraphic framework of the United Kingdom's oil and gas fields. In: Gluyas, J.G., Hichens, H.M. (Eds.), United Kingdom Oil and Gas Fields, Commemorative Millennium Volume. Geological Society, London, Memoirs 20, 17–59.

Wiprut, D., Zoback, M., 2000. Constraining the stress tensor in the Visund field, Norwegian North Sea: Application to wellbore stability and sand production. International Journal of Rock Mechanics and Mining Sciences 37, 317–336.

Wiprut, D., 2001. Stress, Borehole Stability, and Hydrocarbon Leakage in the Northern North Sea. PhD Thesis, Stanford University.

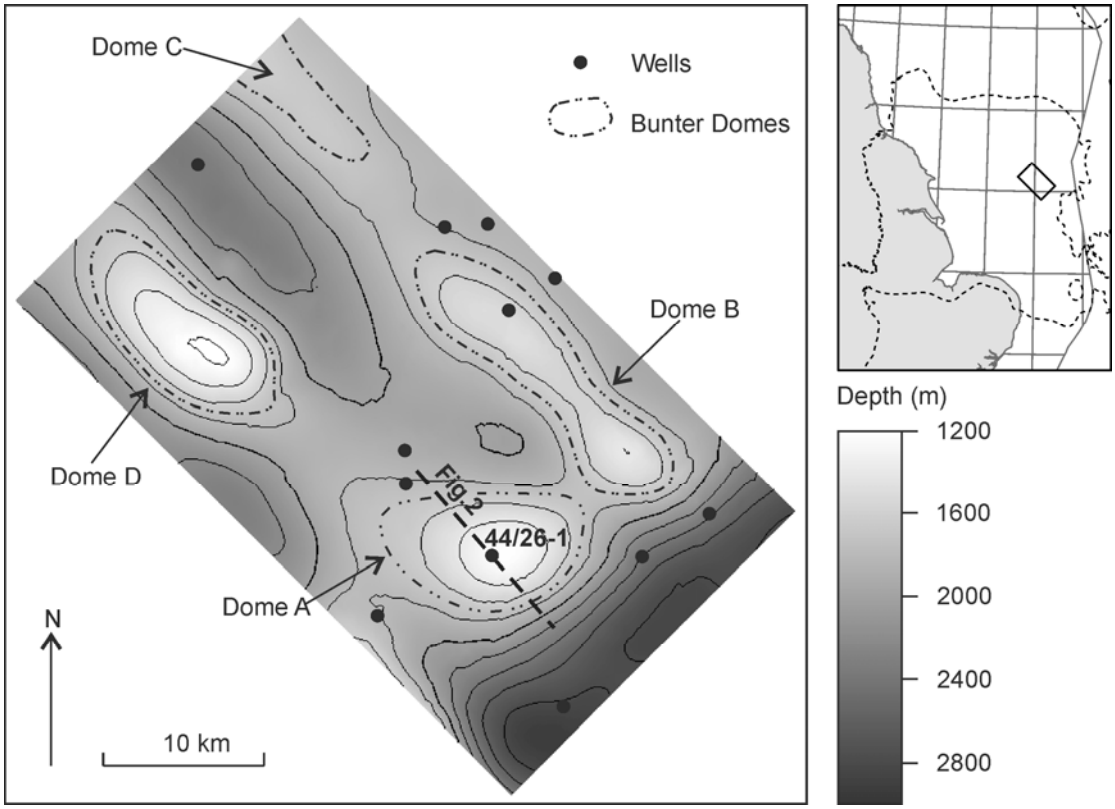

Fig. 1. Depth map (meters sub-sea) of top Bunter Sandstone Formation and location of wells with geophysical logs available for petrophysical analysis. The location of the model area and extent of the Bunter Sandstone Formation in the UK SNS is indicated on the inset map.

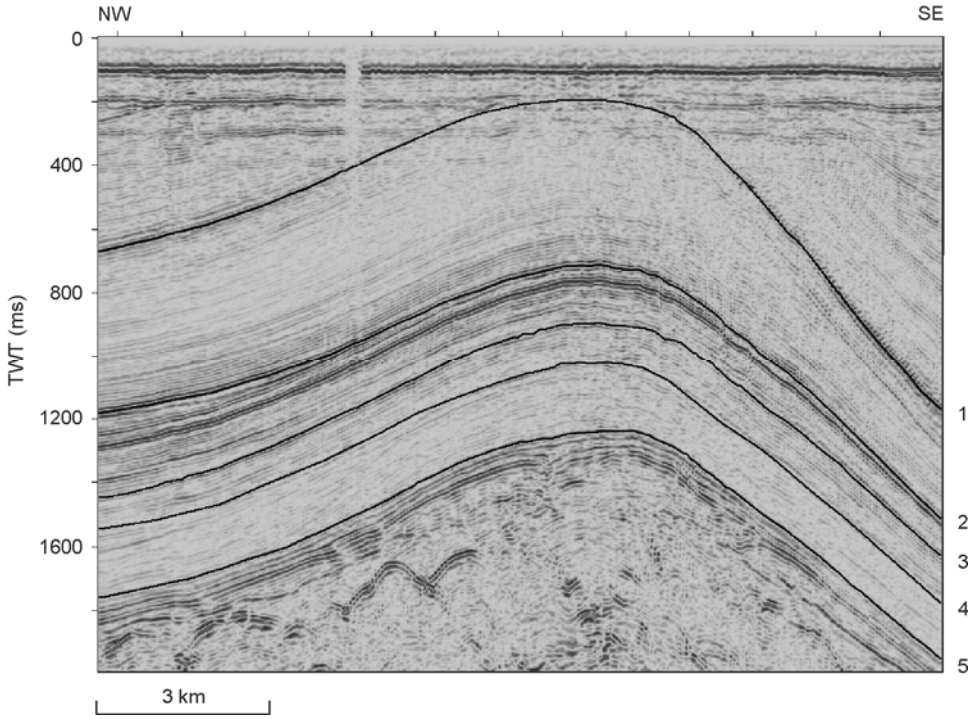

Fig. 2. Seismic reflection section across Dome A. Location of section is marked on Fig. 1. Interpreted reflections are noted on right-hand side of image; (1) top Chalk Group, (2) Base Cretaceous Unconformity, (3) top Bunter Sandstone Formation, (4) near top Bunter Shale Formation and (5) top Zechstein Group. SNS MegaSurvey data courtesy of PGS.

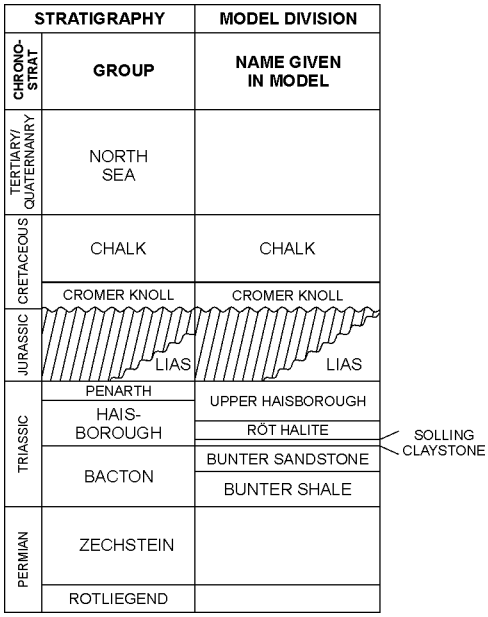

Fig. 3. Generalised stratigraphy of SNS Blocks 44/26 and 44/27 applicable to the Bunter Sandstone Formation 3D reservoir model (left panel), and simplified division as used in the 3D model area. Chalk, Cromer Knoll and Lias groups are included for geological context, and are inactive in the simulation model.

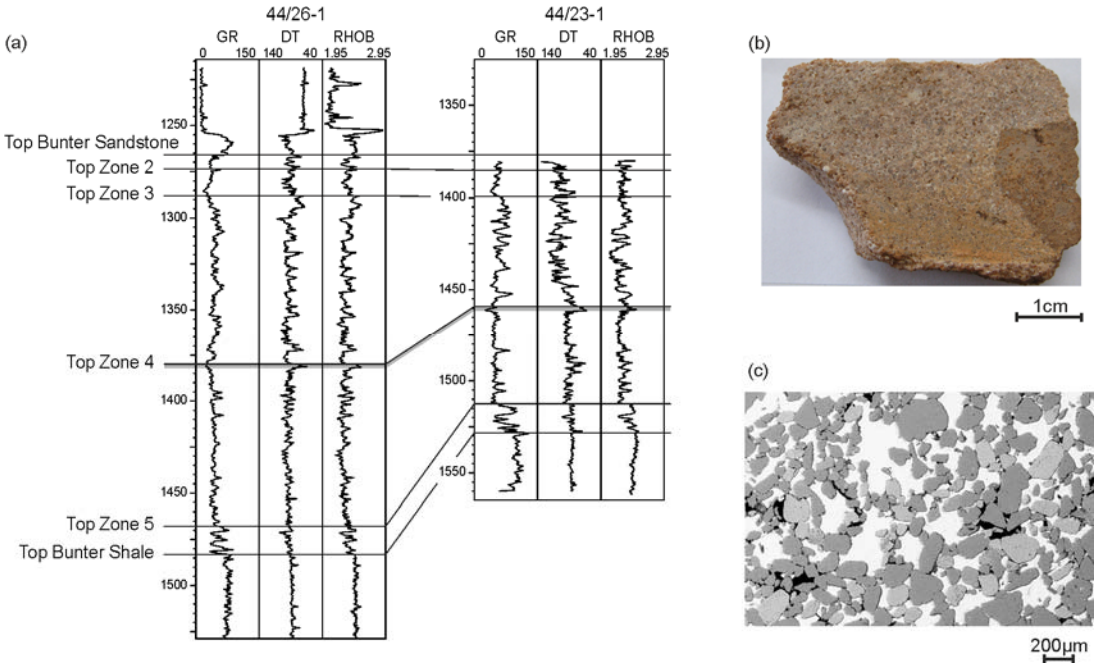

Fig. 4. (a) Well correlation from the model area (44/26–1) to the Caister B gas field (44/23–1). Cemented layer at top of Zone 4 is highlighted in grey. Depths are measured depth. (b) Rock sample from cemented sandstone layer at top of Zone 4 in well 44/23–1 (core sample depth 1458 m). Porosity is occluded by anhydrite cement. (c) SEM image of cemented sandstone at top of Zone 4 in well 44/23–1 (core sample depth 1459 m). The white intra-granular areas are halite cement which almost totally occludes the pore space.

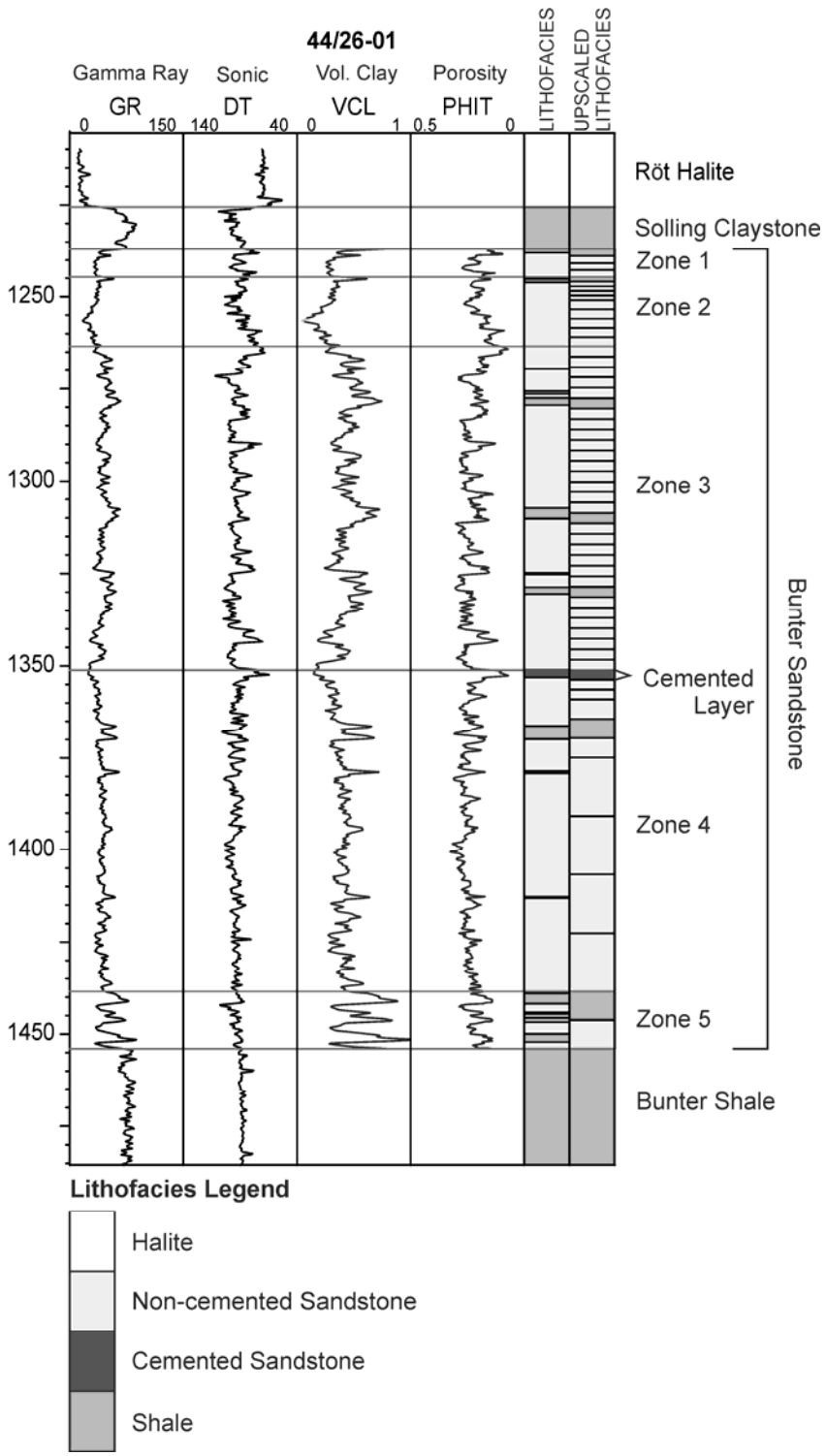

Fig. 5. Relationship between zones, grid layering and upscaled logs. The first lithology track has been interpreted from wireline logs, while the second indicates the grid layering to which the logs have been upscaled.

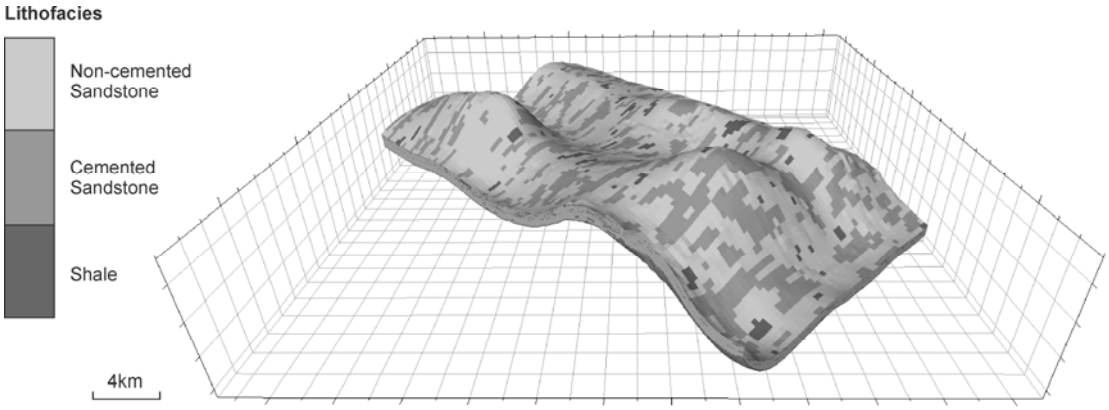

Fig. 6. Perspective view of the static model from the south, showing Bunter Sandstone lithofacies distribution. Vertical exaggeration x5.

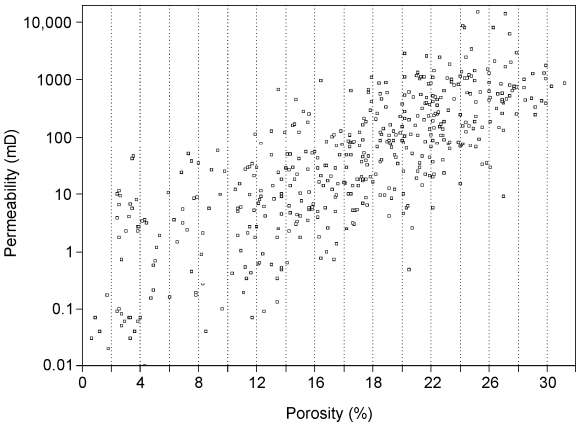

Fig. 7. Cross-plot correlation between porosity and permeability for all available Bunter Sandstone core plugs in the UK sector of the SNS. The vertical lines indicate the porosity binning intervals used by the bivariate SGS algorithm to provide permeability ranges for the different porosity values in the grid.

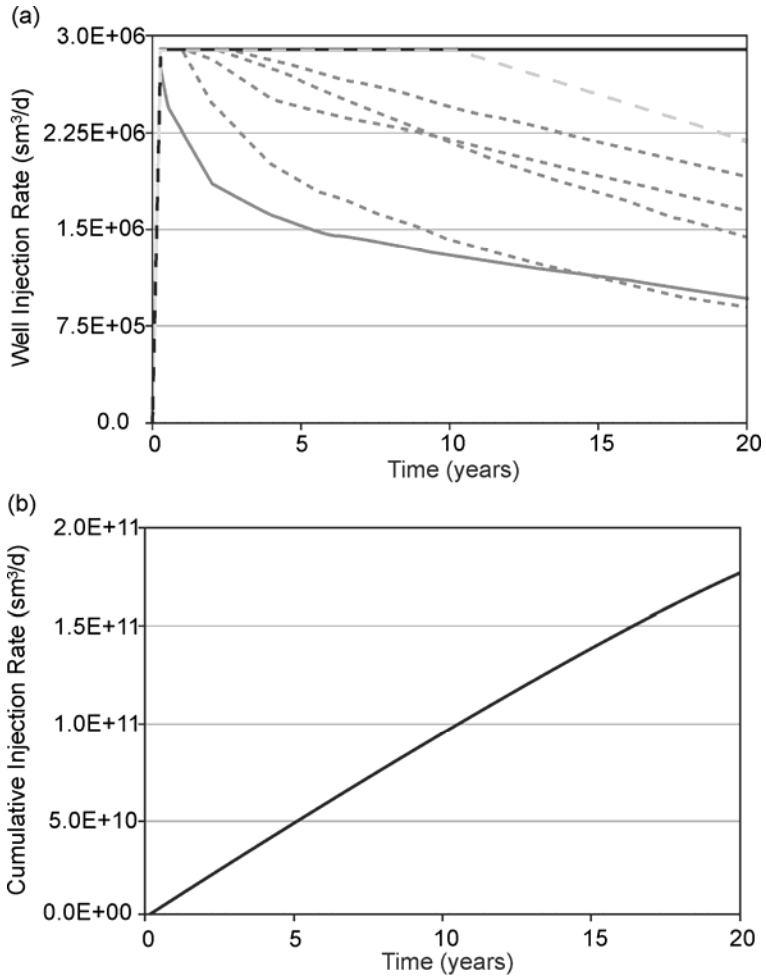

Fig. 8. (a) Injection rate vs time for each well, showing the effect of BHP control. Only four out of ten wells maintained the specified rate of 2.9E+06 sm^3/day (black line at 2.9E+06). In one well the rate was reduced almost immediately (solid grey line) while in four wells the rate was reduced within 2–4 years (dotted lines). The injection rate was maintained in one well for 12 years (dashed grey line). (b) Cumulative injection rate over time.

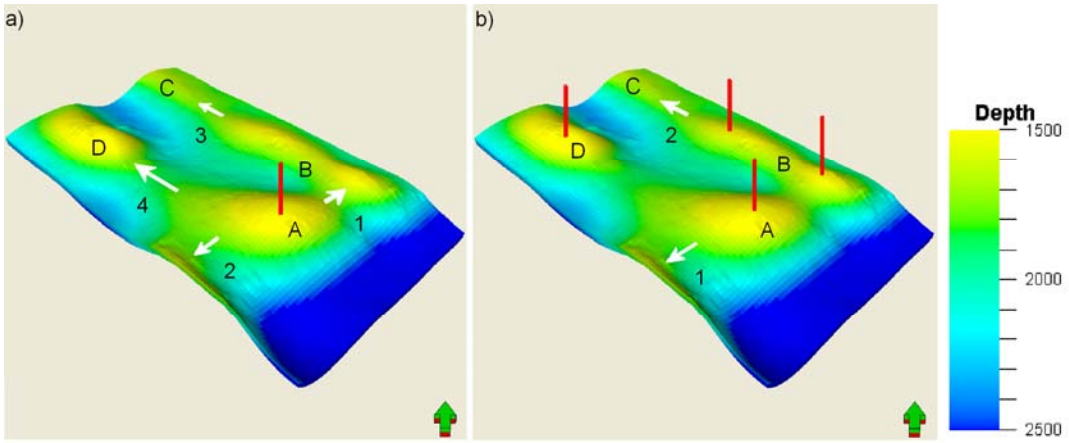

Fig. 9 (a) Spill point directions where injection is considered in Dome A only. (b) Spill point directions where Domes A, B and D are considered as the storage complex. The numbers beside the arrows show the order in which spill points are breached. (Note: Diagram shows only single wells in the domes, whereas 10 injection wells were located in each dome. In the case of Dome B, there were two sets of 5 wells).

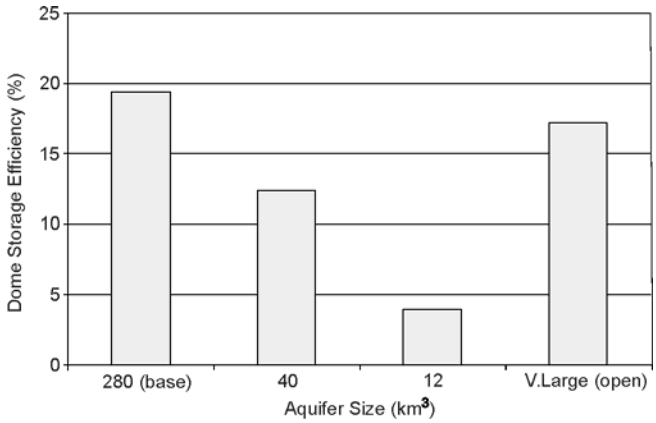

Fig. 10. The effect of total aquifer pore volume on the storage efficiency of Dome A.

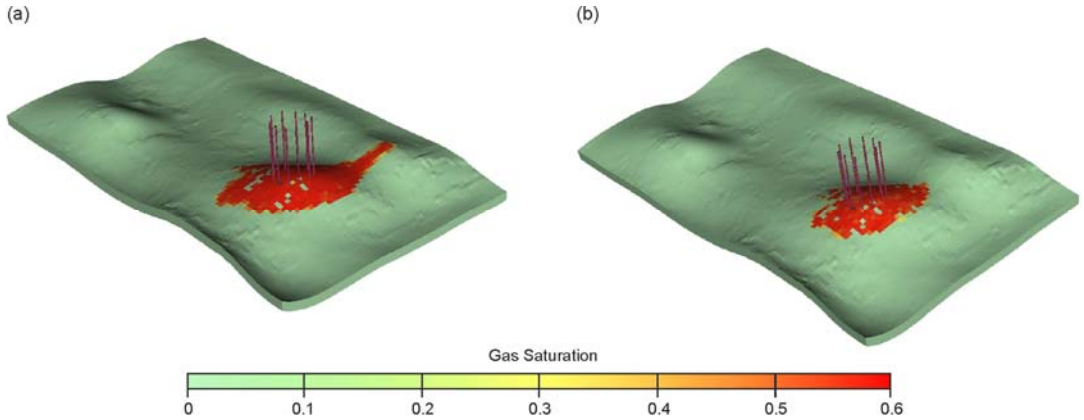

Fig. 11 Perspective view (looking north) showing the CO_2 distribution in the layer immediately beneath the cemented layer after 50 years of injection, for a) the base case and b) the case without the cemented sandstone layer.

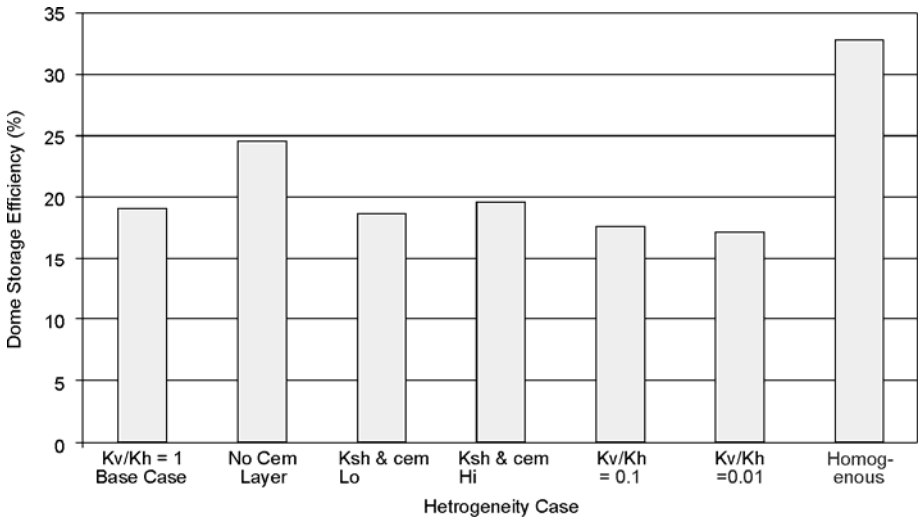

Fig. 12 The effect of heterogeneity on the dome storage efficiency. See text in Section 5.2 for explanation of case names.

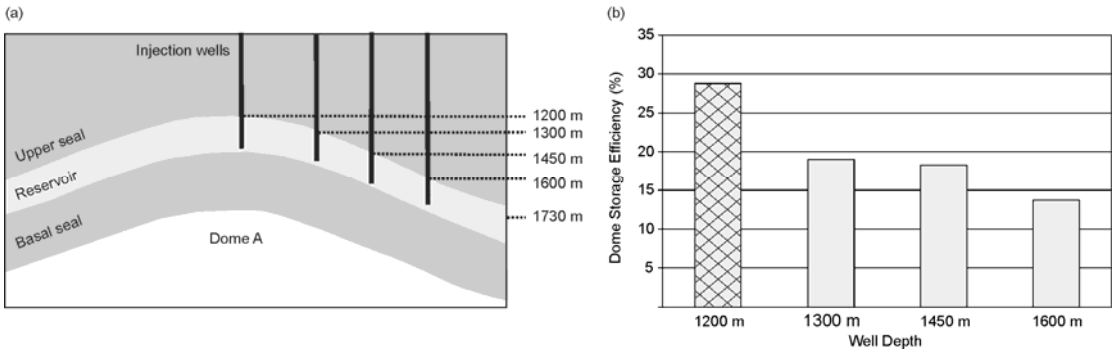

Fig. 13. a) SW-NE schematic cross-section through the model showing different well depths. b) The effect of well placement depth on the dome storage efficiency of Dome A.

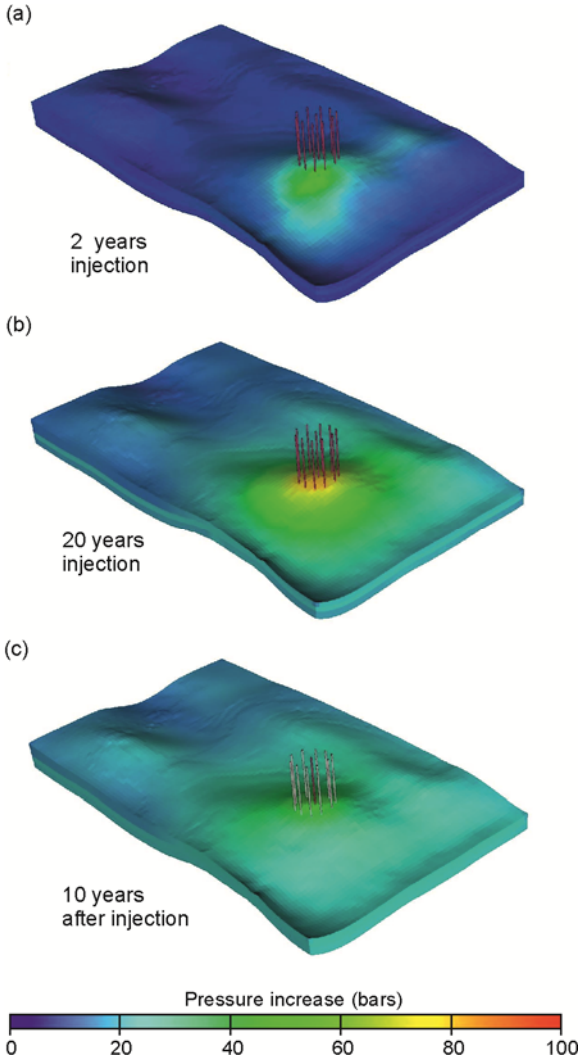

Fig. 14 Perspective view towards north, showing the base case pressure increase due to injection in Dome A after (a) two and (b) 20 years of injection, and (c) 10 years post-injection.

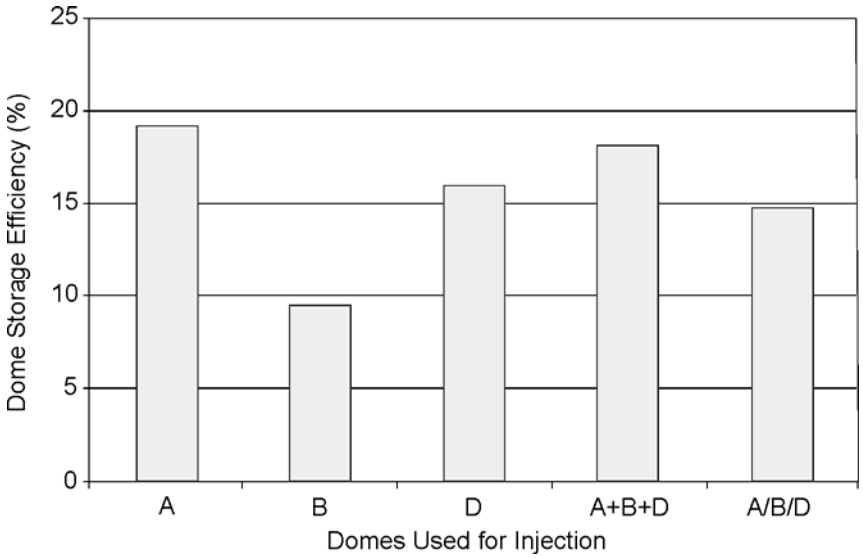

Fig. 15. The effect on storage efficiency of CO_2 injection into multiple domes.

Table 1. Interpreted depositional environment for the Bunter Sandstone zones.

	Interpreted depositional environment	Lithology
Zone 1	Distal flood plain setting with intermittent channels	Dominantly shaley with a marked increase of cemented sandstone layers
Zone 2	Distal flood plain setting with some channels	Shales interbedded with channel sandstones. Increasing shale content in the upper part of the zone. Greater abundance of cemented sandstone layers relative to Zone 3
Zone 3	Cyclic system of braided river channels with sheetflood deposits	Sandstone interbedded with thin shales
Zone 4	Sheetflood dominated	Dominantly sandstone, interbedded with discontinuous shale layers. A 1–2 m thick cemented sandstone bed exists at the top of the zone
Zone 5	Basal progradational sheetflood complex	50% Sandstone, 50% shale

Table 2. Techniques used during lithological modelling of the Bunter Sandstone reservoir zones.

	Technique	Rationale and results
Zone 1	Stochastic Truncated Gaussian Simulation	Elongate variograms trending in sediment transport direction Vertical variogram range of 2 m assigned to represent the rapid vertical variation in lithology
Zone 2	Stochastic object modelling	Channel orientation reflects the likely direction of sediment transport from the southwest towards the northeast Cemented sandstones added as elongate elliptical features orientated in this direction
Zone 3	Stochastic object modelling	Abundance of sandstone channels distributed within a background of shale, with channel orientation reflecting the likely direction of sediment transport Cemented sandstones included as a series of elongate elliptical features oriented concordantly with channel geometries to represent the preferentially cemented coarse-grained channel sands
Zone 4	Stochastic object modelling and log correlation	Low sinuosity channels trending along the direction of sediment transport from southwest make up 97.5% of the volume (observed on upscaled logs) Channels exhibit variable width and thickness, representing sheetflood nature of the sandstones resulting in a scattered distribution of isolated shales trending southwest to northeast Cemented sandstone layer at top of zone manually painted across the model, except in regions around the two wells where it was not observed
Zone 5	Log correlation	Upper shale package and lower sandstone package correlated using geophysical logs.

Table 3. Additional properties used in the simulation model.

Parameters	Units	Value	Reference
Rock compressibility	1/MPa	5.5675×10^{-4}	UK SAP
Water compressibility	1/MPa	3.1325×10^{-4}	UK SAP
Brine salinity range	ppm	130,000–200,000	Bentham, 2006 Smith et al., 2010
Brine viscosity	cp	0.39	UK SAP
Temperature gradient	C/km	36.5	UK SAP
Sea bed temperature	C	4	UK SAP
Pressure gradient	MPa/km	10.07	UK SAP

Lithostatic pressure	MPa/km	22.5	UK SAP
Fracture pressure/initial pressure	dimensionless	1.4	Bentham, 2006
Average porosity in boundary aquifers	m^3/m^3	0.2	Smith et al., 2010
Average permeability in boundary aquifers	mD	100	UK SAP Smith et al., 2010
Aquifer pore volume	km^3	280 in base case	UK SAP

Table 4. Porosity and permeability of the cemented sandstones and shale in the sensitivity studies.

Facies	Base-case poro (%)	Base-case perm (mD)	Ksh&cem hi poro (%)	Ksh&cem hi perm (mD)	Ksh&cem lo poro (%)	Ksh&cem lo perm (mD)
Cemented Sandstone	$1.0E^{-05}$	$6.5E^{-03}$	5	1.0	0.0	0.0
Shale	3	$6.5E^{-03}$	5	1.0	0.0	0.0

Table 5. Summary of the results for the single dome study (Dome A).

Simulation Case	Aquifer PV ($x10^9$ m^3)	Spill time (yrs)	Dome Storage Eff. (%)	Capacity (Mt)
Base-Case	280	20	19.1	331
Closed Aquifer	40	50	12.2	209
Closed Dome	12.2	50	3.9	70
Open Aquifer	24293	16	16.9	290
No Cem Layer	280	26	24.5	426
Ksh&cem lo	280	20	18.8	328
Ksh&cem hi	280	20	19.7	344
Kv/kh 0.01	280	22	17.2	297
Kv/kh 0.1	280	20	17.6	303
Homo	280	42	32.8	484
W1200	280	46	28.7	501
W1450	280	16	18.4	318
W1600	280	12	13.8	237

Table 6. Summary of the results for the multi-dome study. *Note that the pore volume quote here is for the volume above the spill point only.

Simulation Case	Pore Volume ($x10^9$ m^3)	Spill time (yrs)	Dome Storage Eff. (%)			PV-weighted Average (%)	Capacity (Mt)
			A	B	D		
A only*	2.542	20	19.1	-	-	-	331
B only	3.747	12	-	9.4	-	-	242
D only	3.787	26	-	-	15.9	-	413
A+B+D	10.076	100	27.9	9.1	20.5	18.1	1288
A/B/D	10.076	100	19.1	15.3	11.2	14.7	1030